

Apparent fracture toughness of Si_3N_4 -based laminates with residual compressive or tensile stresses in surface layers

M. Lugovy ^{a,*}, V. Slyunyayev ^a, N. Orlovskaya ^b, G. Blugan ^c, J. Kuebler ^c, M. Lewis ^d

^a Institute for Problems of Materials Science, 3 Kzhizhmovski St., 03142 Kiev, Ukraine

^b Drexel University, Philadelphia, USA

^c EMPA, Duebendorf, Switzerland

^d University of Warwick, Coventry, UK

Received 18 December 2003; received in revised form 17 September 2004; accepted 20 September 2004
Available online 28 October 2004

Abstract

The effect of macroscopic residual stresses on the fracture resistance and stable/unstable crack growth in $\text{Si}_3\text{N}_4/\text{Si}_3\text{N}_4$ -30 wt% TiN layered ceramics has been investigated. The laminates were manufactured using rolling and hot pressing techniques. An apparent fracture toughness K_{app} was calculated as a function of the crack length parameter $\tilde{a} = Y(\alpha)a^{1/2}$ for the laminates with residual compressive or tensile stresses in the top layers. The toughness increases in the layers with a compressive stress with increasing crack length, and it decreases in the layers with a tensile stress as the crack continues to grow. An explanation for the experimentally measured and calculated K_{app} values is proposed. The existence of the threshold stress and the stable/unstable crack growth conditions is discussed.

© 2004 Acta Materialia Inc. Published by Elsevier Ltd. All rights reserved.

Keywords: A. Layered structures; B. Fracture toughness; Modeling; C. Crack; Residual stress

1. Introduction

Ceramic matrix composites have a broad range of industrial applications. They have been extensively used as structural components in order to improve the mechanical, thermal and chemical performance of engineering devices. However, despite a high hardness, an excellent oxidation resistance, and high temperature stability, ceramics are inherently brittle. One of the strategies to decrease brittleness and improve composite performance is through the design of ceramic laminates [1]. In recent years, a number of papers have been published on laminates with weak interfaces for crack deflection [2], surface compressive stress [3], crack bifur-

cation in layers with a bulk residual compression [4], phase transformation of zirconia grains under loading [5], and compositional gradient [6–8].

The mismatch of thermal expansion coefficients between different layers inevitably generates thermal residual stresses during subsequent cooling of layered ceramics with strong interfaces [9]. The relative thickness of different layers determines the relative magnitudes of compressive and tensile stress, while the strain mismatch between the layers dictates the absolute values of the residual stresses.

A residual compression of layers results in laminates toughening, which is a crack shielding phenomenon [10]. It has been shown that a residual compression of ~500 MPa in a surface layer of a three-layered alumina–zirconia composite can increase the fracture toughness by a factor of 7.5 (up to 30 MPa m^{1/2}) for crack lengths equal to the surface layer thickness [3]. This mechanism is

* Corresponding author. Tel.: +38 44 457 4890; fax: +38 44 296 1684/380 44 444 21 31.

E-mail address: lugovy@viptelecom.net (M. Lugovy).

associated with the closure stress field behind the crack tip, which is similar to a crack bridging phenomenon acting in non-layered ceramics [11]. However, a toughening by the residual compressive stress is determined by the overall crack length [12], while the toughening by the crack bridging depends only on the length increment of the moving crack. Crack bridging can provide increased toughening by a factor of approximately 2 [11]. Therefore, the residual compressive stresses can provide a significant increase in a ceramic's toughness.

Although fracture toughness of layered composite can be measured experimentally, it is an apparent value because of the superposition of different effects like stress shielding and intrinsic properties of the structure, such as grain size, composition, interfaces, etc. In fracture mechanics, both residual and applied stresses are usually included in the crack driving force. However it can be useful to consider residual stresses as part of the crack resistance. Thus, in laminates with residual compressive stress, the higher resistance to failure results from a reduction of crack driving force rather than from an increase in the intrinsic material resistance to crack extension [12].

A number of the symmetrical layered structures have already been considered in relevant publications [3,5,10]. However, real laminates show some asymmetry of their architecture due to random deviations during the fabrication process. Sometimes the asymmetrical layered structure is designed to meet specific engineering requirements. Another problem is that only a few authors have considered the effect of elastic moduli mismatch between layers on toughening and fracture behavior [13,14]. It was shown that in order to obtain the higher resistance to failure, the tensile layer should be made as stiff as possible (i.e. a high elastic modulus), whereas the compressive layers should be as compliant as feasible (i.e. a low elastic modulus) [14]. However, the conditions of stable or unstable crack growth in ceramic laminates have not been considered in [13,14].

The effect of the residual stress on the apparent fracture toughness and crack growth in non-symmetric Si_3N_4 -based layered composites is analyzed in this study. Special attention is paid to analytical modeling to estimate the fracture toughness as a function of crack length in laminates having different elastic moduli of layers. The validity of the method is examined by a comparison of calculated and measured fracture toughness values. Crack propagation behavior for laminates with the residual compressive or tensile stress in top layers is investigated as well.

2. Experimental

The manufacturing steps of Si_3N_4 -TiN based laminates included (a) ball milling of powders in certain proportions; (b) rolling of thin tapes; (c) hot pressing of

tapes. Two compositions of layers were used: (1) Si_3N_4 (M11, Stark, Germany), (2) Si_3N_4 -30 wt% TiN (grade C, Stark, Germany). The silicon nitride was used with 2 wt% Al_2O_3 and 5 wt% Y_2O_3 additives.

The mixtures of various compositions were milled in the ball mill for 5 h. The average grain size of the milled powders was about 1 μm . Crude rubber (4 wt%) was added to the mixture of powders as a plasticizer through a 3% solution in petrol. The powders were then dried, leaving 2 wt% residual amount of petrol in the mixture. After sieving powders with a 500 μm sieve, granulated powders were dried to 0.5 wt% residual petrol. A roll mill with 40 mm rolls was used for rolling. The velocity of rolling was 1.5 m/min. The working pressure was about 10 MPa to obtain a relative tape density of 64%. The thickness of green tapes was 0.4–0.5 mm and the width was 60–65 mm. Green tapes were stacked together to form the desired layered structures and ceramic samples were prepared by hot pressing the stacked tapes. The hot pressing was performed at 1820 °C and 30 MPa for 45 min without a protective atmosphere.

Both monolithic and layered samples were produced. The monolithic samples were fabricated from stacked tapes of the same Si_3N_4 or Si_3N_4 -30 wt% TiN compositions. Layered samples were prepared using two different designs. The first type of specimen was with the outer layers in residual compression (Si_3N_4 layers); the second type of specimen was with the outer layers in residual tension (Si_3N_4 -30 wt% TiN layers). The laminate parameters, such as composition and thickness of layers, and calculated bulk residual stresses are presented in Table 1. The deviation in the measured thickness of the layers was about 5%. Though both monolithic and layered samples have been nominally prepared from materials of the same grades using the same manufacturing techniques, in reality the samples were prepared from different batches of similar compositions and therefore certain variations between impurities, defects, and other parameters were expected to exist.

The specimens for mechanical tests were prepared by machining the hot pressed tiles. Standard MOR bars of dimensions 50 × 4 × 3 mm were surface ground to the specification stated in EN843-1. The bars were also chamfered along the long edges with a chamfer angle at 45° to a dimension of 0.12 ± 0.03 mm. The fracture toughness was measured by the single edge V-notch beam (SEVNB) technique [15,16] using Eq. (1). The V-notches with a tip radii of an order of 10–15 μm were made in the specimen with a diamond saw, followed by a stainless steel blade notching, and finally a diamond abrasive to obtain a sharp tip for the notch. The elastic modulus was measured by a standard four-point bending technique.

The coefficients of thermal expansion (CTE) of the monolithic materials were measured using 50 mm long MOR bars with a Baehr Dil 802 dilatometer from room temperature to 1100 °C in a nitrogen/hydrogen atmos-

Table 1
Geometrical characteristics of $\text{Si}_3\text{N}_4/\text{Si}_3\text{N}_4\text{-30 wt\% TiN}$ layered materials

Layer #	Specimens of type 1			Specimens of type 2		
	Composition	Layer thickness (μm)	Residual stress (MPa) ^a	Composition	Layer thickness (μm)	Residual stress (MPa) ^a
1	Si_3N_4	752	-223.6	$\text{Si}_3\text{N}_4\text{-30 wt\% TiN}$	852	42.3
2	$\text{Si}_3\text{N}_4\text{-30 wt\% TiN}$	618	186	Si_3N_4	142	-274
3	Si_3N_4	181	-225.7	$\text{Si}_3\text{N}_4\text{-30 wt\% TiN}$	611	44.1
4	$\text{Si}_3\text{N}_4\text{-30 wt\% TiN}$	625	184.4	Si_3N_4	145	-272.5
5	Si_3N_4	176	-227.3	$\text{Si}_3\text{N}_4\text{-30 wt\% TiN}$	611	45.6
6	$\text{Si}_3\text{N}_4\text{-30 wt\% TiN}$	626	182.7	Si_3N_4	143	-271.1
7	Si_3N_4	176	-228.8	$\text{Si}_3\text{N}_4\text{-30 wt\% TiN}$	616	47.1
8	$\text{Si}_3\text{N}_4\text{-30 wt\% TiN}$	620	181.1	Si_3N_4	143	-269.6
9	Si_3N_4	726	-230.9	$\text{Si}_3\text{N}_4\text{-30 wt\% TiN}$	733	48.7
Thickness (μm)	4500			4000		

^a The average residual stress in layer.

phere at a pressure of 10 Pa to avoid oxidation and dissociation of the materials. An analysis of the macrostructure of the specimens was made with an optical microscope.

3. Measurements of the CTEs, the E_i and the $K_{Ic}^{(i)}$ of monolithic ceramics

The values of the thermal expansion coefficient β of the Si_3N_4 and $\text{Si}_3\text{N}_4\text{-30 wt\% TiN}$ monolithic ceramics as a function of temperature are presented in Fig. 2. The CTEs of both compositions are a linear function of the temperature, and the CTE of the $\text{Si}_3\text{N}_4\text{-30 wt\% TiN}$ is higher than the CTE of the Si_3N_4 over all investigated temperature ranges. The temperature dependence of β [K^{-1}] can be presented as $\beta \times 10^6 = 1.09274 \times 10^{-1} + 3.62797 \times 10^{-3}T$ and $\beta \times 10^6 = 1.979406 + 3.02463 \times 10^{-3}T$ for the Si_3N_4 and the $\text{Si}_3\text{N}_4\text{-30 wt\% TiN}$, respectively. The accuracy of such measurements is about 15%.

Young's moduli of the Si_3N_4 and the $\text{Si}_3\text{N}_4\text{-30 wt\% TiN}$ monolithic samples were measured to be 308 and 323 GPa, respectively. Mean values of the intrinsic fracture toughness of monolith materials, measured by SEVNB, are approximately the same for both the Si_3N_4 and the $\text{Si}_3\text{N}_4\text{-30 wt\% TiN}$ compositions, about $4 \pm 1 \text{ MPa m}^{1/2}$. These measured values of CTEs, E_i and $K_{Ic}^{(i)}$ were used in all calculations.

4. Calculation of the apparent fracture toughness

A weight function analysis has been used to estimate the apparent fracture toughness in laminates with residual stresses [3,13,17,18]. A schematic presentation of a two-component multilayered sample is shown in Fig. 1(a), where t_i is the thickness of a i th layer, w is the total thickness of the specimen, b is the width, and N is the total number of layers. The choice of coordinate system is of great importance to the apparent fracture

toughness K_{Ic} calculations because of a significant simplification of the procedure. The most appropriate coordinate origin is on the tensile surface of the sample

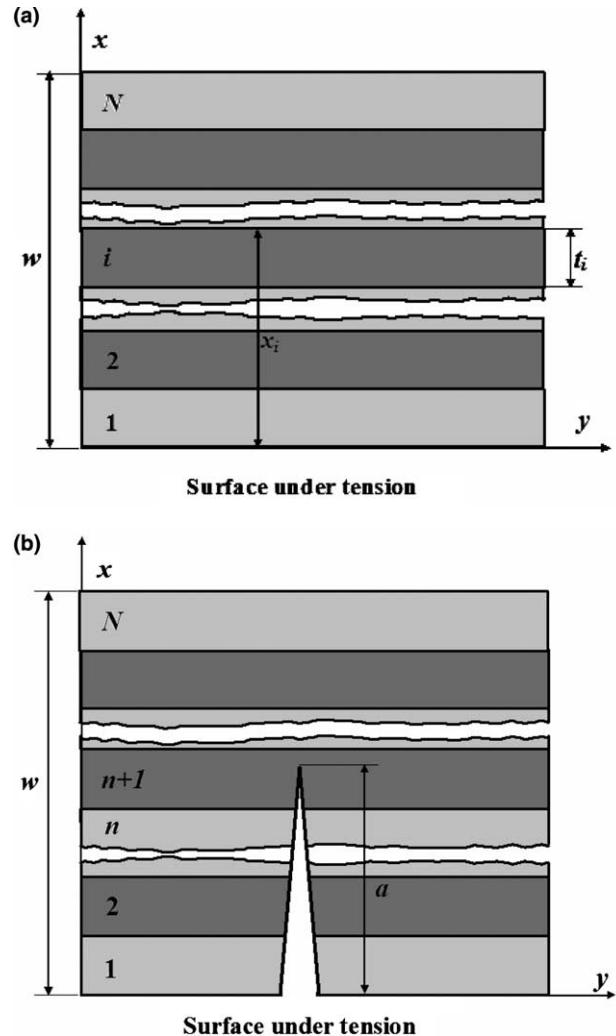


Fig. 1. Scheme of a two-component multilayer specimen: (a) numbers of layers and layer boundary coordinates; (b) an analyzed crack location in a layered sample.

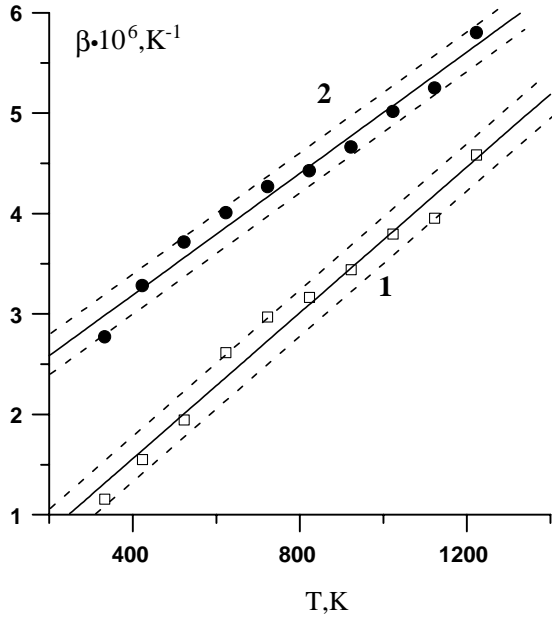


Fig. 2. Thermal expansion coefficients (CTEs) of the Si_3N_4 (1) and the Si_3N_4 -30 wt% TiN (2) in the 290–1200 K temperature range. Dashed lines show experimental range of CTEs.

under bending. The geometry of the multilayered material analyzed here is such that the problem can be reduced to one dimension and that analytically tractable solutions can be used [18]. A schematic presentation of the analyzed crack location in the layered specimen is presented in Fig. 1(b), where a is the crack length and n is the number of layers crossed by the crack.

An experimental value of the apparent fracture toughness can be found using the expression [19]:

$$K_{\text{app}} = Y(\alpha)\sigma_m a^{1/2}, \quad (1)$$

where

$$Y(\alpha) = \frac{1.99 - \alpha(1 - \alpha)(2.15 - 3.93\alpha + 2.7\alpha^2)}{(1 + 2\alpha)(1 - \alpha)^{3/2}},$$

$$\sigma_m = \frac{1.5P(s_1 - s_2)}{bw^2} \quad \text{and} \quad \alpha = a/w,$$

where P is the critical load (the applied bending load corresponding to specimen failure) and s_1 and s_2 are outer and inner support spans of the four-point bending fixture for SEVNB samples.

The apparent fracture toughness of the layered composite can be calculated analytically by [18]:

where $K_{1c}^{(i)}$ is the intrinsic fracture toughness of the i th layer material, K_r is the stress intensity due to the residual stresses, $h(x/a, \alpha)$ is the weight function for an edge-cracked sample [13,17,18], x_i is the coordinate of an upper boundary of the i th layer (Fig. 1), $E_i' = E_i/(1 - \nu_i)$, and E_i and ν_i are the elastic modulus and Poisson ratio of the i th layer, respectively. A Poisson ratio of 0.25 for both compositions was used in all calculations. The expressions for I_{Lj} ($j = 0, 1, 2$) and J_{Lj} ($j = 0, 1$) were obtained in [18] as follows:

$$I_{Lj} = \frac{1}{j+1} \sum_{i=1}^N E_i'(x_i^{j+1} - x_{i-1}^{j+1}), \quad (3)$$

$$J_{Lj} = \frac{1}{j+1} \sum_{i=1}^N \tilde{\epsilon}_i E_i'(x_i^{j+1} - x_{i-1}^{j+1}), \quad (4)$$

where $\tilde{\epsilon}_i$ is the strain in the i th layer, which is not associated with any stress. The thermal expansion and/or volume change due to a crystallographic phase transformation might be the source of this strain. However, the case of a phase transformation is out of the scope of this paper. In the case of thermal expansion:

$$\tilde{\epsilon}_i = \int_{T_0}^{T_j} \beta_i(T) dT,$$

where $\beta_i(T)$ is the thermal expansion coefficient of the i th layer at the temperature T . T_0 and T_j are the actual and “joining” temperatures, respectively. During sample cooling, the strain mismatch due to the different thermal expansion coefficients is accommodated by creep as long as the temperature is high enough. Below a certain temperature, called the “joining” temperature, the different components become bonded together and residual stresses appear. The “joining” temperature is difficult to measure experimentally, and in general, T_j is adopted to be somewhere below the sintering temperature. If $\beta_i(T)$ is a linear function, $\tilde{\epsilon}_i = \langle \beta_i \rangle \Delta T$, where $\Delta T = T_j - T_0$, $\langle \beta_i \rangle = \frac{\beta_i(T_0) + \beta_i(T_j)}{2}$ is the average value of the thermal expansion coefficient in the temperature range from T_0 to T_j . Other authors [20] used ~ 1200 K as the “joining” temperature for calculation of the residual stresses of Si_3N_4 based laminates. However, in our case, 948 and 765 K were assumed for ΔT with the laminates with compressive and tensile residual stresses in the top layers, respectively, because these temperatures provided the best fit between the calculated and experimentally measured values of fracture toughness for both types of laminate.

$$K_{\text{app}} = \frac{6Y(\alpha)a^{1/2}(I_{L1}^2 - I_{L0}I_{L2})(K_{1c}^{(i)} - K_r)}{w^2 \left\{ E_{n+1}' \int_{x_n}^a h\left(\frac{x}{a}, \alpha\right) [I_{L0}x - I_{L1}] dx + \sum_{i=1}^n E_i' \int_{x_{i-1}}^{x_i} h\left(\frac{x}{a}, \alpha\right) [I_{L0}x - I_{L1}] dx \right\}}, \quad (2)$$

The stress intensity due to the residual stresses is [18]:

$$K_r = \frac{1}{I_{L1}^2 - I_{L0}I_{L2}} \left\{ E'_{n+1} \int_{x_n}^a h\left(\frac{x}{a}, \alpha\right) \times [I_{L1}J_{L1} - I_{L2}J_{L0} + (I_{L1}J_{L0} - I_{L0}J_{L1})x] dx + \sum_{i=1}^n E'_i \int_{x_{i-1}}^{x_i} h\left(\frac{x}{a}, \alpha\right) [I_{L1}J_{L1} - I_{L2}J_{L0} + (I_{L1}J_{L0} - I_{L0}J_{L1})x] dx \right\}. \quad (5)$$

The apparent fracture toughness K_{app} in layered specimens can be analyzed as a function of the crack length parameter \tilde{a} , where $\tilde{a} = Y(\alpha)a^{1/2}$. The crack length parameter \tilde{a} is the most appropriate to demonstrate critical conditions of a crack growth. One of the advantages of this parameter is that the stress intensity factor of an edge crack for a fixed value of the applied stress σ_m is a straight line from the coordinate origin in the coordinate system $K_{app}-\tilde{a}$. Since $K_1 = \sigma_m \tilde{a}$, the slope of the straight line is the applied stress σ_m . The conditions for unstable crack growth in the internal stress field are as follows [12]: $K_1(\sigma_m, a) = K_{app}(a)$; $dK_1(\sigma_m, a)/da \geq dK_{app}(a)/da$. Using parameter \tilde{a} , these conditions become $\sigma_m \tilde{a} = K_{app}(\tilde{a})$ and $\sigma_m \geq dK_{app}(\tilde{a})/d\tilde{a}$, which can be reduced to:

$$K_{app}(\tilde{a})/\tilde{a} \geq dK_{app}(\tilde{a})/d\tilde{a}. \quad (6)$$

It follows from Eq. (6) that unstable crack growth occurs if the slope of the straight line corresponding to the stress intensity factor at constant applied stress is greater than or equal to the slope of the tangent line to the fracture resistance curve at the same point (Fig. 3). Also the applied stress intensity factor becomes higher than the fracture resistance of the material.

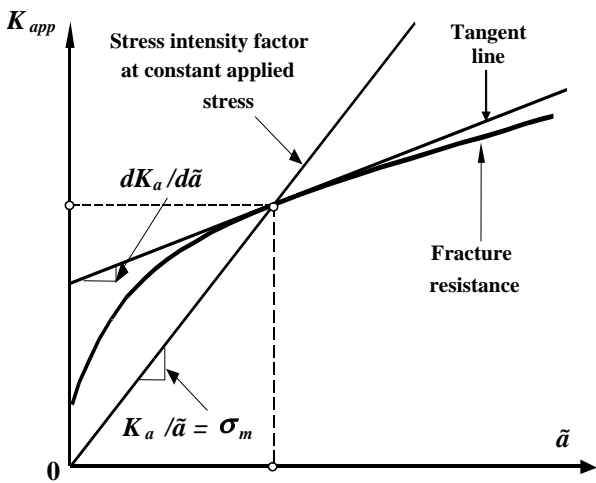


Fig. 3. General criterion of stable/unstable crack growth in a brittle material.

5. Apparent fracture toughness of the layered composite with residual compressive or tensile stresses in the top layer

The calculated values of the apparent fracture toughness as a function of the crack length parameter \tilde{a} in the $\text{Si}_3\text{N}_4/\text{Si}_3\text{N}_4-30 \text{ wt}\% \text{ TiN}$ laminate with compressive outer layers are shown in Fig. 4(a). The toughness increases in the layers with compressive stress with increasing crack length, and it decreases in the layers with tensile stress as the crack continues to grow. The layers with compressive and tensile stresses are

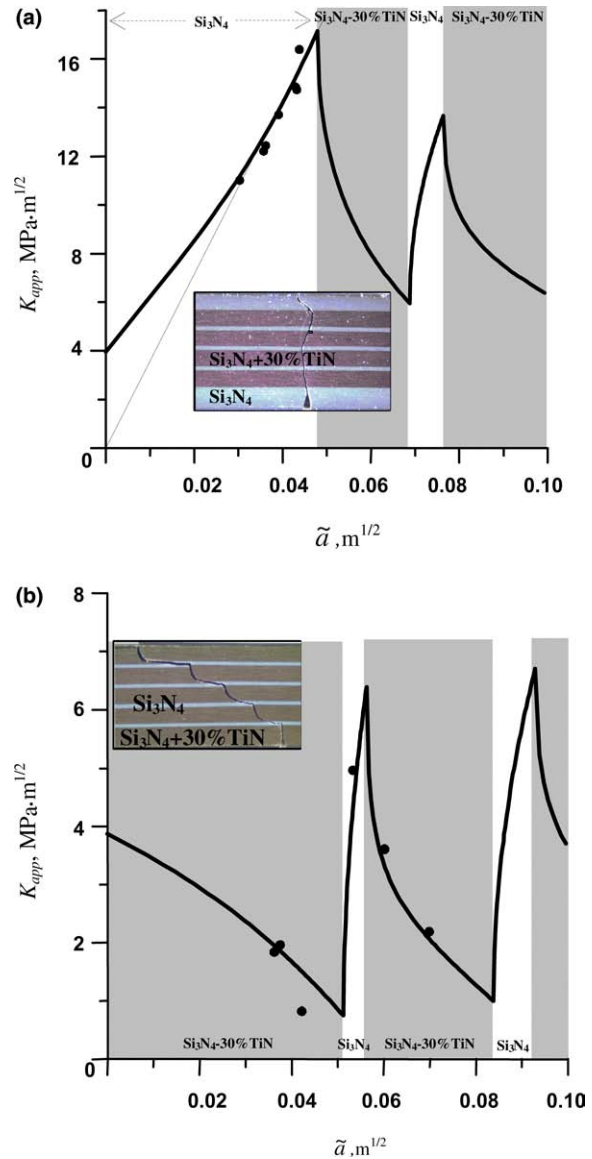


Fig. 4. The apparent fracture toughness as a function of the crack length parameter \tilde{a} in the laminate with compressive (a) and tensile (b) outer layers. Filled circles correspond to the experimental data. Inserts are optical micrographs of the two parts of $\text{Si}_3\text{N}_4/\text{Si}_3\text{N}_4-30 \text{ wt}\% \text{ TiN}$ laminate samples with (a) Si_3N_4 surface layers with a residual compressive stress and (b) $\text{Si}_3\text{N}_4-30 \text{ wt}\% \text{ TiN}$ surface layers with a residual tensile stress after SEVNB test.

shown in Fig. 4 in white and gray colors, respectively. As one can see, K_{app} reaches its maximum or minimum values as the crack approaches the interface with a new layer of an opposite stress sign. For the first Si_3N_4 top layer with compressive stress, the calculated apparent fracture toughness increases from 3.9 to 17 $\text{MPa m}^{1/2}$ as a function of the crack length parameter. The experimentally measured K_{app} values, presented as solid circles in Fig. 4(a), show an excellent fit with the calculated values. The crack length parameters for the experimentally measured K_{app} were calculated from the initial notch lengths. All experimentally measured points are located on close to a straight line between the coordinate origin and the maximum K_{app} point at the interface between the first and second layers. The failure of all samples occurred at 351 ± 13 MPa. The calculated K_{app} decreases in the second Si_3N_4 -30 wt% TiN layer with a residual tensile stress from 17 to 5 $\text{MPa m}^{1/2}$, followed by the next increase from 5 to 14 $\text{MPa m}^{1/2}$ in the third Si_3N_4 layer with a residual compressive stress. The insert in Fig. 4(a) shows an optical micrograph of two parts of the $\text{Si}_3\text{N}_4/\text{Si}_3\text{N}_4$ -30 wt% TiN laminate sample with a V-notch in the top layer with residual compressive stress after the SEVNB test. As one can see, there is a relatively straight crack path with no sharp crack deviation, deflection, or bifurcation during the crack propagation.

Fig. 4(b) shows the calculated apparent fracture toughness as a function of the crack length parameter \bar{a} in the $\text{Si}_3\text{N}_4/\text{Si}_3\text{N}_4$ -30 wt% TiN laminate with a residual tensile stress in the outer layers. The toughness decreases from 3.9 to 0.8 $\text{MPa m}^{1/2}$ within the first Si_3N_4 -30 wt% TiN layer as the crack reaches the first interface. Toughness increases from 0.8 to 6.4 $\text{MPa m}^{1/2}$ in the second Si_3N_4 layer with a residual compressive stress, and it decreases again from 6.4 to 1 $\text{MPa m}^{1/2}$

within the third Si_3N_4 -30 wt% TiN layer with a residual tensile stress. There is no continuous growth of the crack in this case. The crack starts to propagate, then becomes arrested, after this it continues to grow again. The crack arrest results in a “pop-in” event at the load–displacement diagram (Fig. 5). A stress of such “pop-in” event is the onset stress of crack propagation. This stress, as well as an initial notch length was used to calculate the measured apparent fracture toughness. Experimentally measured values of K_{app} fit well with the calculated numbers. The experimental data can be considered to be two different sets. The first set includes the K_{app} measured with notch tips within the first Si_3N_4 -30 wt% TiN and the second Si_3N_4 layers. The failure of all samples from the first set occurred at 116.2 MPa. The second set includes two K_{app} values measured with notch tips within the third Si_3N_4 -30 wt% TiN layer. The failure of these two samples occurred at 71 ± 1 MPa. The insert in Fig. 4(b) shows an optical micrograph of two parts of the $\text{Si}_3\text{N}_4/\text{Si}_3\text{N}_4$ -30 wt% TiN laminate sample with the V-notch placed in the Si_3N_4 -30 wt% TiN top layer with a residual tensile stress after the SEVNB test. As one can see from the optical image, the crack path deviates strongly from a straight line with 90° crack deflection occurring in the center of each Si_3N_4 layer with a residual compressive stress. While traveling only a short distance of about a Si_3N_4 -30 wt% TiN layer thickness along a centerline, the crack kinks out into the Si_3N_4 -30 wt% TiN layer with a residual tensile stress.

6. Discussion

The calculations indicate an unambiguous trend for the apparent fracture toughness behavior. The K_{app} increases in the layers with a residual compressive stress and decreases in the layers with a residual tensile stress

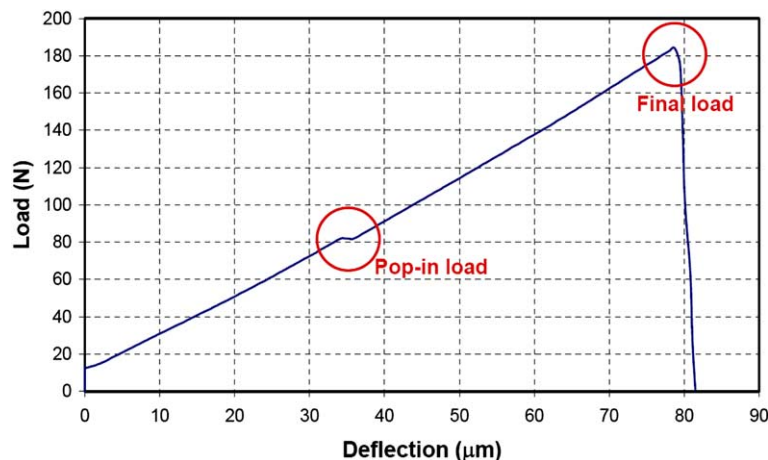


Fig. 5. Load–displacement diagram of SEVNB sample with pop-in.

as a function of the crack length (or the crack length parameter). The calculated increase of K_{app} is confirmed by the experimental data in the laminates with the compressive outer layer (Fig. 4(a)). As one can see from Fig. 6(a), the cracks that have the crack length parameter from O to the point A_1 will demonstrate an unstable crack growth. In this case, once the crack started to propagate at a certain stress, it cannot be arrested; this results in complete failure of the sample, since the applied stress intensity factor is always higher than a fracture resistance of the laminate. The cracks that have the crack length parameter between the point A_1 and the point A_3 will propagate in two stages. For example,

the crack with the crack length parameter A_2 will have an unstable growth from the point B_2 to the point C on the K_{app} - \tilde{a} plot (Fig. 6(a)). The stable growth of this crack will occur from the point C to the point D . For all cracks with a crack length parameter \tilde{a} from the point A_1 to the point A_4 , the failure occurs at the stress equal to the slope of the OD straight line, which is a threshold stress. The threshold stress σ_{thr} is determined by the maximum value of K_{app} at the interface between the first (compressive) and the second (tensile) layers, and no failure can occur below the σ_{thr} if the sample contains the surface cracks located only in the first layer. The curvature of the K_{app} plot is a function of a value of the residual stress. The higher residual stress, the more concave the curvature of K_{app} is. At a certain small value of a residual compressive stress, the line OD can have only one intersection point with K_{app} plot, and therefore no stable crack growth stage can occur.

The conditions of the stable/unstable crack growth in the laminate with residual tensile stress in top layer are shown in Fig. 6(b). The crack with a crack length parameter A_1 for such laminates will propagate only unstably at the stress level above σ_{OB1} . The crack with the crack length parameter A grows unstably at the stress σ_{OB} . This unstable growth occurs between points B and C (Fig. 6(b)), because the points belonging to the BC segment lie above the K_{app} plot. At point C , the condition of the Eq. (6) is violated and the crack growth becomes stable between points C and D , which means that any crack advancement requires an increase of the applied stress. Point D is a maximum value of K_{app} at the interface between the second (compressive) and the third (tensile) layers. This point determines a stress $\sigma_{OD} = \sigma_{thr}$. Above σ_{OD} , the crack propagates unstably up to a complete failure. In such a way all initial cracks in the first (tensile) and the second (compressive) layers with a crack length parameter greater than A_2 (Fig. 6(b)) will initiate the specimen failure at the same $\sigma_{OD} = \sigma_{thr}$ stress value. The initial cracks with tips in the third and the fourth layers will initiate specimen failure at the different stress value that is determined by the maximum value of the K_{app} at the interface between the fourth and the fifth layers. This stress is σ_{thr} for cracks with tips located in the third and the fourth layers. It should be noted that points the B or B_3 in Fig. 6(b) correspond to the measured K_{app} values (using “pop-in” stress), while the points B' or B'_3 belonging to the OD straight line are determined by the initial notch length and the failure stress of the sample.

As implied by the above analysis, the surface cracks which have sufficient length to fall into the region of a stable crack growth will all cause a failure at the same σ_{thr} stress. At the same time, if a residual compressive stress in the top layer is not high enough, the small cracks can cause catastrophic failure once they start to grow. Therefore, it might be that different mechanisms

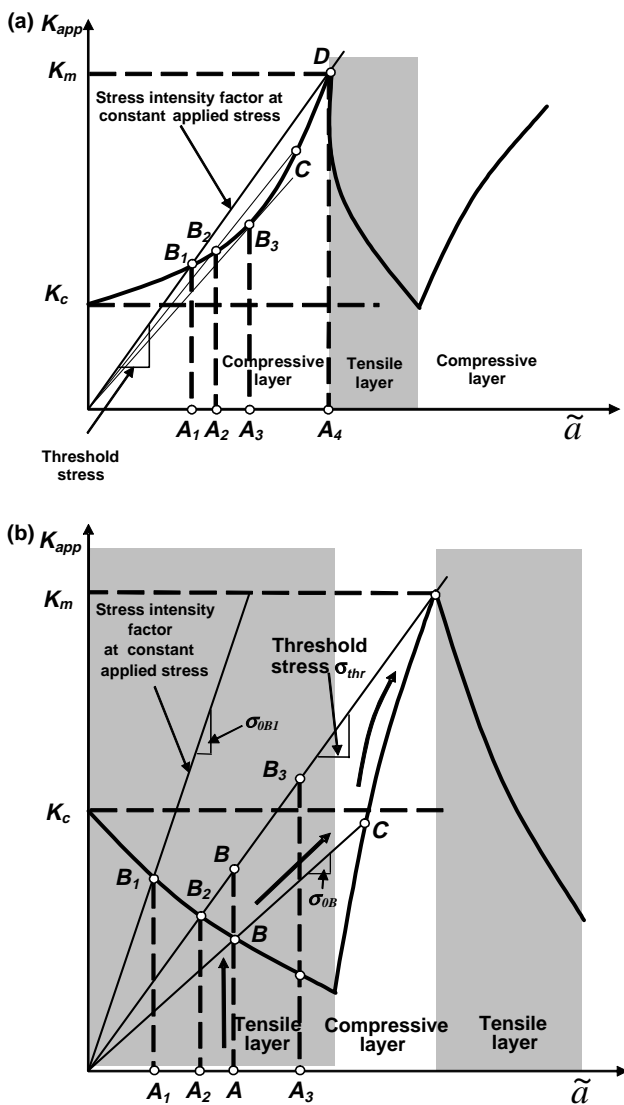


Fig. 6. Conditions for stable/unstable crack growth in a layered structure: (a) a range of crack length parameters for stable crack growth in a laminate with a residual compressive stress in a top layer; (b) stable/unstable crack growth in a laminate with a residual tensile stress in a top layer.

such as a crack bridging or transformation toughening can be more effective at preventing small cracks from growing unstably.

7. Conclusions

The apparent fracture toughness as a function of the crack length parameter $\tilde{a} = Y(\alpha)a^{1/2}$ has been calculated for the $\text{Si}_3\text{N}_4/\text{Si}_3\text{N}_4\text{-30 wt\% TiN}$ laminates with residual compressive or tensile stresses in the top layers. The toughness increases in the layers with a compressive stress as the crack length increases, and it decreases in the layers with a tensile stress as the crack continues to grow. The experimentally measured K_{app} values for the laminates show an excellent fit with the calculated values. It was found that a threshold stress exists for cracks of a certain length. Stable crack growth occurs for the majority of cracks with a threshold stress as indicated by the $K_{\text{app}}\text{-}\tilde{a}$ graph. The cracks with a small length will propagate unstably because the applied stress intensity factor is always higher than a fracture resistance of the laminate.

If the residual compressive stress is small enough, the situation can occur where no stable crack growth exists for cracks with tips located within the first compressive layer. Therefore, it is important to introduce high residual compressive stresses that will provide a steep slope of the apparent fracture toughness curve to include cracks of a short length in the region of stable crack growth. Obtaining a high residual compressive stress in the first layer is an effective way of providing high toughness at small crack lengths, thereby ensuring the improved flaw tolerance and surface damage resistance.

Acknowledgement

The work was supported by the European Commission. It is a part of the Project 1CA2-CT-2000-10020 Copernicus-2 “Silicon nitride based laminar and func-

tionally gradient ceramics for engineering application”. EMPA was funded in this project by BBW, the Swiss Federal Office for Education and Science, under contract number 99.0785.

References

- [1] Chan M. *Ann Rev Mater Sci* 1997;27:249.
- [2] Clegg WJ, Kendall K, Alford NMcN, Button TW, Birchall JD. *Nature* 1990;347:455.
- [3] Lakshminarayanan R, Shetty DK, Cutler RA. *J Am Ceram Soc* 1996;79(1):79.
- [4] Lugovy M, Orlovskaya N, Slyunyayev V, Gogotsi G, Kuebler J, Sanchez-Herencia AJ. *Comp Sci Technol* 2002;62:819.
- [5] Marshall DB, Ratto JJ, Lange FF. *J Am Ceram Soc* 1991;74(12):2979.
- [6] Finot M, Suresh S, Giannakopoulos AE. *Proc Int Symp Struct Func Grad Mater* 1995;3:223.
- [7] Yoo J, Cho K, Bae WS, Cima M, Suresh S. *J Am Ceram Soc* 1998;81(1):21.
- [8] Thompson SC, Pandit A, Padture NP, Suresh S. *J Am Ceram Soc* 2002;85(8):2059.
- [9] Lugovy M, Orlovskaya N, Berroth K, Kuebler J. *Comp Sci Technol* 1999;59:1429.
- [10] Blattner AJ, Lakshminarayanan R, Shetty DK. *Eng Fract Mech* 2001;68:1.
- [11] Evans AG. *J Am Ceram Soc* 1990;73(2):187.
- [12] Sglavo VM, Larentis L, Green DJ. *J Am Ceram Soc* 2001;84(8):1827.
- [13] Moon RJ, Hoffman M, Hilden J, Bowman K, Trumble K, Roedel J. *J Am Ceram Soc* 2002;85(6):1505.
- [14] Hbaieb K, McMeeking RM. *Mech Mater* 2002;34:755.
- [15] Kuebler J. *Ceram Eng Sci Proc* 1997;18:155–62.
- [16] Kuebler J. ASTM STP 1409, J.A. Salem. In: Jenkins MG, Quinn GD, editors. ASTM, West Conshohocken, PA, USA, ISBN 0-8031-2880-0; 2002. p. 93.
- [17] Fett T, Munz D. *J Mater Sci Lett* 1990;9:1403.
- [18] Lugovy M, Slyunyayev V, Subbotin V, Orlovskaya N, Gogotsi G. *Comp Sci Technol* 2004;64:1947.
- [19] Srawley JE. *Int J Fract* 1976;12:475.
- [20] Sajgalik P, Lences Z, Dusza J. Factors influencing the residual stresses in layered silicon nitride based composites. In: *Engineering Ceramics'96: Higher reliability through processing*, NATO ASI series. 3. High Technology, vol. 25. Dordrecht: Kluwer Academic Publishers; 1997. p. 301.